Coalescence of Au Nanoparticles without Ligand Detachment

Pan Guo[1] and Yi Gao[1,2,*]

[1]Division of Interfacial Water and Key Laboratory of Interfacial Physics and Technology, Shanghai Institute of Applied Physics, Chinese Academy of Sciences, Shanghai 201800, China
[2]Shanghai Advanced Research Institute, Chinese Academy of Sciences, Shanghai 201210, China

(Received 4 April 2019; revised manuscript received 7 November 2019; accepted 15 January 2020; published 11 February 2020)

Repulsion of ligands is known as the key factor for hindering nanoparticle (NP) coalescence. Thus, during the past decade, it has generally accepted that the full removal of capping ligands of the contact surface is the first step for NP coalescence. Herein, using molecular dynamics simulations, we have identified a new mechanism for the coalescence of $S(CH_2)_nCOOH$-coated Au NPs in water without ligand detachment. In contrast to the traditional mechanism, the aggregation of the NPs is induced by the twined hydrophobic chains of the ligands rather than the hydrophilic carboxyl tails as believed previously. Next, the exposed surface atoms attach to form the neck, and extend with the atomic rearrangement of the contact interface to merge the NPs, which do not need the removal of ligands as expected from traditional supposition. This finding refreshes the understanding of the atomic mechanism of the coalescence of NPs, which paves the way for the rational design and synthesis of NPs.

DOI: 10.1103/PhysRevLett.124.066101

The growth of metal nanoparticles (NPs) via merging of primary particles has been of wide interest owing to its ubiquity in crystallization and assembly processes [1–3]. The morphology and size of NPs are key factors affecting their electrical, optical, or catalytic properties [4–6]. Hence, understanding the merging mechanism of NPs is of fundamental importance for the synthesis of NPs with controllable size and structures for practical applications [7–9], including energy conversion, catalysis, bioimaging, and sensor development.

Coalescence, as one of the most common merging processes, has been widely studied in the past decades [1,10,11]. Generally, it starts with the formation of a connective neck and extends the contact area to a larger individual particle [12–18]. However, owing to the limitation of *in situ* liquid-cell electron microscopy techniques [10], whether and how the contact interface (i.e., surface atoms of NPs, ligands, and the neighboring water molecules) varies during coalescence has not been identified yet [1,19]. In particular, previous theoretical and simulation studies focused on the uncoated NPs though [12,14,20–25] the coalescence mechanism of the ligands-coated NPs are rarely studied, which hinders the full understanding of the atomic mechanism of the merging process.

During the past decades, it was accepted that molecular ligands serve as stabilizers to prevent nanoparticle merging, and contribute to superlattice formation via ligand interdigitation [26–28]. Thus, the full removal of capping ligands of the contact surface was generally believed to be the first step of merging of NPs [13,15,29]. However, it should be noted that removal of ligands requires relatively higher temperature [30,31]. Interestingly, recent experiments have reported the extensive evidences of the spontaneous merging of thiol-capped Au NPs under ambient condition at room temperature [4,32,33], in which condition the ligands can hardly be removed. This arouses the confusion of the traditional coalescence mechanism [34,35].

Here, based on molecular dynamics (MD) simulations, we have identified a new mechanism for the coalescence of $S(CH_2)_nCOOH$-coated Au NPs in water without ligand detachment. Contrary to the traditional assumption that interdigitation of ligands occupy the interval of pairing ligand-coated NPs and obstruct the merging of NPs, we find that ligands prefer twining the surface of not fully coated NPs. The hydrophobic interaction between the chains of ligands induces the aggregation of the Au NPs and further attachment via the exposed surface atoms. During the coalescence process, the atomic rearrangement of the contact interface repels the ligands out from the interval of NPs. Our new findings show the removal of ligands is not necessary for the coalescence of Au NPs, which explains the occurrence of merging of Au NPs at room temperature [4,32,33]. Moreover, the spontaneous expulsion of ligand-coated surface atoms and the reconstruction of the contact interface provides a new understanding of the coalescence process of NPs, which would be beneficial for the tuning of the controllable growth of NPs.

The ligand-coated Au NPs $Au_{147}[S(CH_2)_nCOOH]_{27}$ were constructed with Au_{147} of I_h symmetry and 27 mercaptan acids randomly coated on bridge and atop sites (see PS7 of the Supplemental Material [36]). The corresponding packing density (Σ) of ligands on the surface of

NPs is 4.1 nm^{-2}. The ligands do not fully cover the surface of Au NP, because merging of the not fully coated NPs is ubiquity and has been reported by previous experimental studies [18,52]. We varied the length of the alkyl chains from $n = 1$ to $n = 7$. For SCH_2COOH, packing densities from 4.4, 4.9, 6.7, to 8.5 nm^{-2} were considered with corresponding numbers of ligands of 29, 32, 44, and 56, respectively. The MD simulations were performed to study the coalescence of two NPs in water (see Table S1 in the Supplemental Material [36]). Each system was sampled with 5 independent trajectories. First, a simulation of 10 ns with the position restraint of Au atoms at their original sites was performed to relax the ligands in water. Then the position restraints on the Au atoms were released, and a new simulation of no less than 30 ns was performed to observe the coalescence process of Au NPs. The periodic boundary condition was applied in all directions. The MD simulations were performed using a time step of 1.0 fs with Gromacs 5.0.7 [53] in an *NVT* ensemble with a velocity-rescale thermostat at a temperature of 300 K. In the simulations, the Au atoms were modeled as uncharged Lennard-Jones particles with a cross section of $\sigma_{AuAu} = 0.2629$ nm, and a depth of the potential well of $\varepsilon_{AuAu} = 22.1330$ kJ/mol [37]. The force field parameters for Au and S atoms were from Ref. [37]. The OPLSAA force field [38] was used for the other atoms in ligands (see Table S2 in the Supplemental Material [36]). The SPC/E model [54] was used for the water molecules. The cutoff of 1.2 nm was applied for the van der Waals interactions and the long-range electrostatic interactions using the particle-mesh Ewald (PME) [55] method. Umbrella sampling combined with the weighted histogram analysis method (WHAM) [39,40] were used to calculate the potential of mean force (PMF) of the coalescence process of two Au NPs in water. The separation distance between the center of mass of the two Au NPs (d) was defined to be the reaction coordinate (see Supplemental Material PS3 [36] for detailed PMF calculation methods).

The typical coalescence trajectory of two $Au_{147}(SCH_2COOH)_{27}$ ($\Sigma = 4.1$ nm^{-2}) in water without ligand detachment is shown in Fig. 1(a). To understand the process in detail, the interaction between NPs (E_{tot}, which is divided into three parts, including the interaction from ligands E_{ll}, from Au atoms E_{aa}, and between ligands and

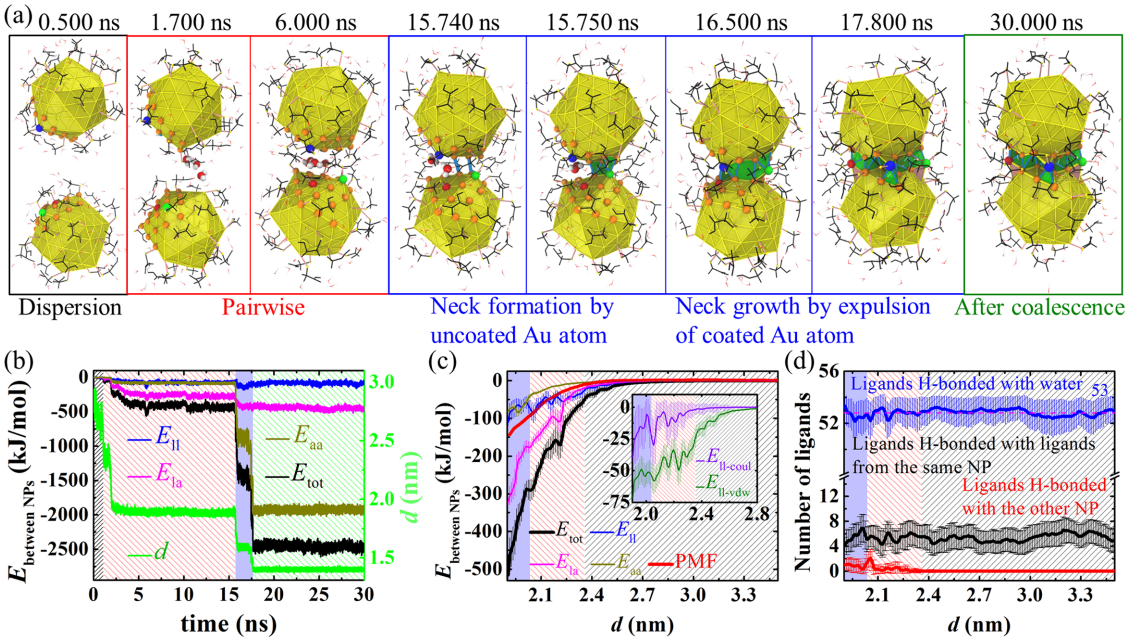

FIG. 1. (a) Snapshots of the coalescence trajectory of two $Au_{147}(SCH_2COOH)_{27}$ ($\Sigma = 4.1$ nm^{-2}) in water. The original NPs are shown in yellow with Au atoms in the final contact interface as orange spheres; among them, the ligand-coated Au atom being expulsed from the contact area as colored spheres and the resulting new surfaces formed by Au atoms from the same NP in pink. The contact area of two NPs is shown as blue lines and green surfaces. (S atom, yellow; Au-S bond, pink; ligands, black; water formed hydrogen bonds (H-bonded) with ligands, red and white; water not H-bonded with ligands are omitted for clear views). (b) The interaction energy between NPs (E_{tot}, black), including the interaction from ligands (E_{ll}, blue), Au atoms (E_{aa}, brown), and between ligands and Au atoms (E_{la}, magenta), together with the separation distance between the center of mass of the two Au_{147} (d, green, right green axis) during the coalescence process. Blue vertical regions indicate the time of coalescence, including neck formation and growth. Black, red, and green shaded areas indicate the states before and after coalescence. (c) Free-energy profile of the coalescence process (PMF, red) in comparison with the interaction energy between NPs. The free-energy profile is defined to zero at $d = 3.5$ nm. E_{ll} is further divided into the van der Waals portion $E_{ll\text{-}vdw}$ (green) and the electrostatic portion $E_{ll\text{-}coul}$ (purple) as shown in the inset. (d) Number of ligand H-bonded with water molecules (blue), with ligands from the same NP (black), and from the other NP (red) as a function of d.

Au atoms E_{la}), as well as the separation distance between the center of mass of the two Au_{147} (d) during the simulation trajectory have been calculated and shown in Fig. 1(b). Initially, NPs are dispersed in water, $E_{tot} \approx 0$ kJ/mol, the radii of Au_{147} and $Au_{147}(SCH_2COOH)_{27}$ in water are $R_{Au147} \approx 0.74 \pm 0.05$ nm and $R_{NP} \approx 1.14 \pm 0.05$ nm, respectively (see Fig. S2 in the Supplemental Material [36]). The ligands are prone to lying on the surface, with thickness of $(L_{ligand}) \sim 0.4$ nm. As the NPs gradually approaching each other, a relatively stable pairwise state is formed with $E_{tot} < -50$ kJ/mol. E_{ll} is comparable to E_{la}, and E_{aa} shows no evident increment with a plateau of d at ~2.36 nm [$\sim (2R_{Au147} + 2L_{ligand})$]. Then, E_{la} increases rapidly compared to E_{ll} and E_{aa}, and becomes dominant in E_{tot}. Simultaneously, d decreases to a new plateau of ~1.89 nm [$\sim (2R_{Au147} + L_{ligand})$].

In the interval of pairing NPs, neck formation begins with atomic-scale attachment of uncoated surface atoms and rapidly expands to other surrounding surface atoms, then temporarily stops at the coated surface atoms. Afterwards, neck growth is accomplished by expulsion of ligand-coated surface atoms from the contact interface. Once the attachment starts, E_{aa} becomes dominant until the end of the simulation. Finally, d is reduced to ~1.4 nm ($\sim 2R_{Au147}$). Thus, the coalescence process can be divided into four steps: diffusion in water, formation of pairwise structure, neck formation and growth, and termination of coalescence.

The driving force of coalescence is further investigated by analyzing the potentials of mean force (PMF) of the coalescence process [Fig. 1(c)]. The PMF is defined to be zero when NPs are dispersed in water. PMF steadily decreases as d decreases, indicating that the coalescence process is dominated by the interaction between the two NPs. Intuitively, acid-coated NPs [56,57] assemble by formation of hydrogen bonds (H-bonds) between COOH groups [50,51]. However, the van der Waals portion of E_{ll} is more dominant than the electrostatic portion in the pairwise state [the inset of Fig. 1(c) and Fig. S3 in the Supplemental Material [36]]. Meanwhile, the number of ligands that H-bonded with water molecules show no obvious change during the coalescence [Fig. 1(d), see Supplemental Material PS6 [36] for a detailed definition of H-bonds]. These results reveal that the hydrophobic interaction between the chains of the ligands dominates the aggregation of the Au NPs.

To uncover the mechanism of neck formation, the variation of the effective radius of NP in water (R_{NP}), the coverage of ligands ($S_{ligands}/S_{NP}$), and the exposure of surface atoms ($S_{Au\_exposed}/S_{Au147}$) with the length of ligands [n for $S(CH_2)_nCOOH$] have been calculated and shown in Fig. 2. Here, S_{NP} represents the solvent accessible surface area (SASA) of NP in water (including two parts, the ligand portion $S_{ligands}$ and the surface atom portion $S_{Au\_exposed}$, $S_{ligands}$ is further divided into the carboxyl tails

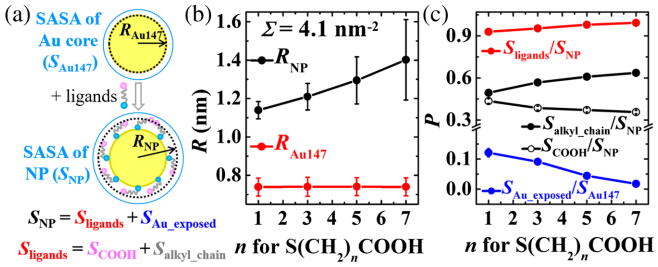

FIG. 2. (a) Scheme for ligands twining the surface of not fully coated NPs. (b) The effective radius of $S(CH_2)_nCOOH$ coated Au_{147} in water (R_{NP}, black) as a function of n, the radii of Au_{147} (R_{Au147}, red) are also shown as a reference. (c) The coverage of ligands ($S_{ligands}/S_{NP}$, red) and the exposure of surface atoms ($S_{Au\ exposed}/S_{Au147}$, blue) on NP in water as a function of n. $S_{ligands}/S_{NP}$ is further divided in to the COOH portion (S_{COOH}/S_{NP}) and the alkyl chains portion ($S_{alkyl\ chian}/S_{NP}$).

portion S_{COOH} and the alkyl chain portion S_{alkyl_chian}), and S_{Au147} is SASA of Au_{147}. Figure 2 shows that R_{NP} increases from 1.14 to 1.40 nm (with 0.26 nm increment) as n increases from $n = 1$ to 7, accompanied with S_{alkyl_chian}/S_{NP} increases and $S_{Au\_exposed}/S_{Au147}$ decrease as n increases. These results imply that ligands prefer twining the surface of not fully coated NPs, and some surface atoms can be exposed for attachment.

To illustrate the molecular mechanism of neck growth, the extension of the contact area accompanied by the rearrangement of the ligand-coated Au atoms and the expulsion of their ligands is shown in Fig. 3(a). During the coalescence process, E_{aa} and d experience stepwise variation [Fig. 3(b)], corresponding to the stepwise reconstruction of the contact interface. First, the rearrangement of the ligand-coated Au atoms 188 together with the

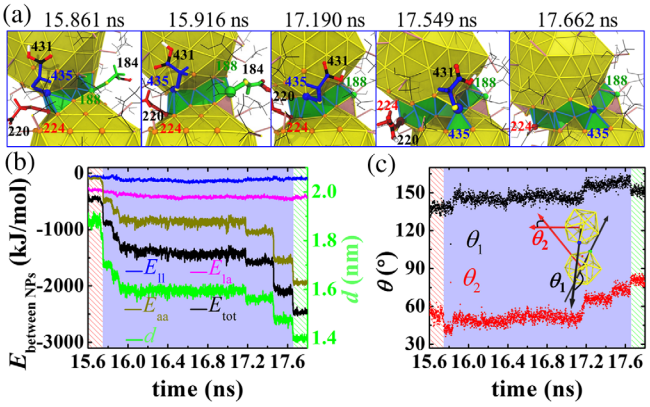

FIG. 3. (a) Snapshots of the rearrangement of the ligand-coated Au atoms during the coalescence process. The expulsed ligands are shown in the same color as the coated Au atoms, other colors used are the same as Fig. 1(a). (b) Enlarged coalescence region in Fig. 1(b). (c) Angles between orientations of different NPs. The value of angle changes as the relative rotation of NPs occurs. The orientations of NPs are defined as two vectors pointing from the center of mass of Au_{147} to two adjacent vertices of Au_{147}.

expulsion of its ligand 184 results in the relative rotation between NPs from 15.861 to 15.916 ns [Fig. 3(c)]. Later, the NPs rotate to adjust their relative orientation to decrease the lattice mismatch within the contact area from 17.170 to 17.190 ns. Then, the rearrangement of the ligand-coated Au atoms 224 and 435, as well as the expulsion of their ligands 220 and 431, occurs from 17.400 to 17.549 ns, followed by the reconfiguration of atoms within the contact area from 17.648 to 17.662 ns. Coalescence stops when the contact area between NPs covers two surfaces of each NP, implying that the original geometry of NPs influences the degree of coalescence. The driving force of the neck growth can be attributed to the reduction of the surface energy to maximize the interaction between Au atoms [1,58]. The relative rotation between NPs is consistent with the *in situ* liquid-cell transmission electron microscopy (TEM) observations that the nanoparticles undergo multiple rotational motions after attachment to minimize the misalignment of their lattices [1,12,16].

In short, we have identified a new mechanism for the coalescence of NPs in water (Fig. 4). First, the hydrophobic interaction between the twined chains of the ligands dominates the aggregation of the Au NPs. Ligands do not fully cover the surface of NPs, which leads to exposure of surface atoms for attachment. Next, the attached interface grows up with the atomic rearrangement of the contact interface to repel the ligands from the interval of the NPs to the surface outside.

The new mechanism we identified shows the removal of ligands is not necessary for the coalescence of Au NPs, which indicates the coalescence can be much easier than thought before and takes place at room temperature [4,32,33]. For example, Kundu *et al.* observed the increase of the size of ligand-coated Au nanoparticles at room temperature from ~2.6 nm to ~4.6 and 11.8 nm by using grazing incidence small angle x-ray scattering techniques [32], which can be well explained by this mechanism.

The influence of the length of ligands on the coalescence of NPs has been examined by increasing the alkyl chains of ligands [$S(CH_2)_nCOOH$] from $n = 1$ to

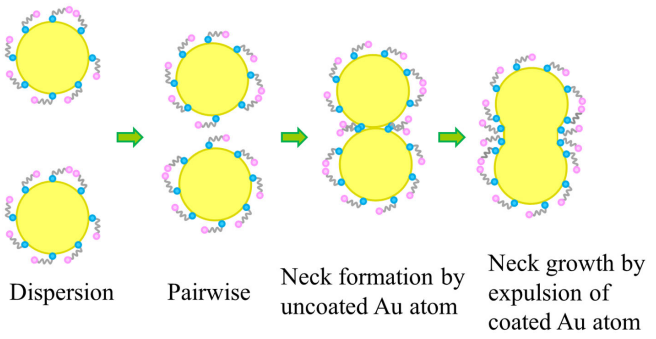

FIG. 4. Scheme for the coalescence mechanism of Au NPs in water mediated by atomic rearrangement of surface atoms without ligand detachment.

$n = 3$, 5, and 7 (see Supplemental Material PS8 [36] for details). This coalescence mechanism (Fig. 4) also applies for $n = 3$. When the length of the ligand is similar to the side length of a single crystal surface of Au_{147} ($L_s \approx 0.89 \pm 0.02$ nm, see Fig. S2 in the Supplemental Material [36]), $n = 5$, ligands in the interval of pairing NPs obstruct the further attachment of NPs to terminate the coalescence of NPs. When the length of the ligand exceeds L_s, $n = 7$, coalescence of NPs is not observed. Therefore, we can reasonably propose that the critical length of ligands hindering the merging of NPs is the length of the longest distance between the vertices of the crystal surface. Interestingly, the separation distance between pairwise Au_{147} changes slightly with the variation of the length of ligands due to the twined alkyl chains of ligands around the NP under the influence of hydrophobic interaction [59,60]. This well explains the spacing between the NPs before pairwise attachment can be much shorter than the length of ligands [29,61].

To show the robustness of the neck growth by expulsion of ligand-coated surface atoms from the contact interface, we have artificially adjusted the well depth of the van der Waals potential, ε_{AuAu}, of Au atoms from $\varepsilon'_{AuAu} = 1.2$ to $2.0\varepsilon_{AuAu}$ (see Supplemental Material PS9 [36] for details). The coalescence of NPs with the expulsion of ligand-coated surface atoms from the contact interface can be observed until $\varepsilon'_{AuAu} = 2.0\varepsilon_{AuAu}$.

The dependence of coalescence on the packing density of NPs is investigated by varying the packing density of SCH_2COOH-coated Au_{147} from 4.4, 4.9, 6.7, to 8.5 nm^{-2} (see Table S4 in the Supplemental Material PS10 [36]). The new mechanism (Fig. 4) applies to NPs with the packing density of 4.4 nm^{-2}, which is slightly lower than that of defect-free alkanethiol SAM with 100% coverage on Au(111) (4.67 nm^{-2}) [48,49]. When the packing density is denser than 4.67 nm^{-2}, i.e., $\Sigma = 4.9$ and 6.7 nm^{-2}, the local packing density increased around the neck to obstruct the further attachment of NPs to terminate the coalescence of NPs. When $\Sigma = 8.5$ nm^{-2}, coalescence of NPs is not observed. In addition, the critical packing density slightly decreases to 4.2 and 4.1 nm^{-2} with an increase in size of the NP to Au_{309} and Au_{561}, respectively (see Table S5 in the Supplemental Material PS11 [36]).

In summary, we have identified a new mechanism for the coalescence of $S(CH_2)_nCOOH$-coated Au NPs in water by the rearrangement of the ligand-coated surface atoms rather than the removal of ligands. Contrary to the traditional assumptions that interdigitation of ligands should be detached completely from the pairing ligand-coated NPs, the new mechanism provides more complexity for the nucleation and growth of the ligand-protected NPs. This study refreshes the conventional understanding of the atomic mechanism of NP coalescence, which lays the foundation for the rational design of functional NPs.

We thank Jinrong Yang for valuable discussions. P. G. thanks the support of the China Postdoctoral Science Foundation funded project (2018M632188). Y. G. thanks for the funding support from the National Natural Science Foundation of China (11574340, 21773287). The computational resources utilized in this research were provided by the Shanghai Supercomputer Center, National Supercomputing Center in Guangzhou (NSCC-GZ) and Tianjin.

*gaoyi@zjlab.org.cn

[1] J. Lee, J. Yang, S. G. Kwon, and T. Hyeon, Nat. Rev. Mater. **1**, 16034 (2016).
[2] J. J. De Yoreo, P. U. P. A. Gilbert, N. A. J. M. Sommerdijk, R. L. Penn, S. Whitelam, D. Joester, H. Zhang, J. D. Rimer, A. Navrotsky, J. F. Banfield, A. F. Wallace, F. M. Michel, F. C. Meldrum, H. Cölfen, and P. M. Dove, Science **349**, aaa6760 (2015).
[3] N. T. Thanh, N. Maclean, and S. Mahiddine, Chem. Rev. **114**, 7610 (2014).
[4] Q. Yao, X. Yuan, V. Fung, Y. Yu, D. T. Leong, D.-e. Jiang, and J. Xie, Nat. Commun. **8**, 927 (2017).
[5] H. Qian, M. Zhu, Z. Wu, and R. Jin, Acc. Chem. Res. **45**, 1470 (2012).
[6] Y. Wu, X. Sun, Y. Yang, J. Li, Y. Zhang, and D. Qin, Acc. Chem. Res. **50**, 1774 (2017).
[7] I. Chakraborty and T. Pradeep, Chem. Rev. **117**, 8208 (2017).
[8] R. Jin, C. Zeng, M. Zhou, and Y. Chen, Chem. Rev. **116**, 10346 (2016).
[9] M.-C. Daniel and D. Astruc, Chem. Rev. **104**, 293 (2004).
[10] B. H. Kim, J. Yang, D. Lee, B. K. Choi, T. Hyeon, and J. Park, Adv. Mater. **30**, 1703316 (2018).
[11] H. Zheng, R. K. Smith, Y.-w. Jun, C. Kisielowski, U. Dahmen, and A. P. Alivisatos, Science **324**, 1309 (2009).
[12] Z. Aabdin, J. Lu, X. Zhu, U. Anand, N. D. Loh, H. Su, and U. Mirsaidov, Nano Lett. **14**, 6639 (2014).
[13] H.-G. Liao, L. Cui, S. Whitelam, and H. Zheng, Science **336**, 1011 (2012).
[14] T. H. Lim, D. McCarthy, S. C. Hendy, K. J. Stevens, S. A. Brown, and R. D. Tilley, ACS Nano **3**, 3809 (2009).
[15] M. A. van Huis, L. T. Kunneman, K. Overgaag, Q. Xu, G. Pandraud, H. W. Zandbergen, and D. Vanmaekelbergh, Nano Lett. **8**, 3959 (2008).
[16] J. M. Yuk, M. Jeong, S. Y. Kim, H. K. Seo, J. Kim, and J. Y. Lee, Chem. Commun. **49**, 11479 (2013).
[17] J. M. Yuk, J. Park, P. Ercius, K. Kim, D. J. Hellebusch, M. F. Crommie, J. Y. Lee, A. Zettl, and A. P. Alivisatos, Science **336**, 61 (2012).
[18] C. S. Sandeep, J. M. Azpiroz, W. H. Evers, S. C. Boehme, I. Moreels, S. Kinge, L. D. Siebbeles, I. Infante, and A. J. Houtepen, ACS Nano **8**, 11499 (2014).
[19] D. Li, M. H. Nielsen, J. R. Lee, C. Frandsen, J. F. Banfield, and J. J. De Yoreo, Science **336**, 1014 (2012).
[20] J. Antúnez-García, S. Mejía-Rosales, E. Pérez-Tijerina, J. M. Montejano-Carrizales, and M. José-Yacamán, Materials **4**, 368 (2011).
[21] M. Lal, M. Plummer, J. Purton, and W. Smith, Proc. R. Soc. A **467**, 1986 (2011).
[22] R. Sathiyanarayanan, M. Alimohammadi, Y. Zhou, and K. A. Fichthorn, J. Phys. Chem. C **115**, 18983 (2011).
[23] D. A. Welch, T. J. Woehl, C. Park, R. Faller, J. E. Evans, and N. D. Browning, ACS Nano **10**, 181 (2016).
[24] J. Wang, S. Chen, K. Cui, D. Li, and D. Chen, ACS Nano **10**, 2893 (2016).
[25] B. Jin, M. L. Sushko, Z. Liu, C. Jin, and R. Tang, Nano Lett. **18**, 6551 (2018).
[26] K. J. Si, Y. Chen, Q. Shi, and W. Cheng, Adv. Sci. **5**, 1700179 (2018).
[27] J. C. Love, L. A. Estroff, J. K. Kriebel, R. G. Nuzzo, and G. M. Whitesides, Chem. Rev. **105**, 1103 (2005).
[28] Z. L. Wang, S. A. Harfenist, I. Vezmar, R. L. Whetten, J. Bentley, N. D. Evans, and K. B. Alexander, Adv. Mater. **10**, 808 (1998).
[29] C. Zhu, S. Liang, E. Song, Y. Zhou, W. Wang, F. Shan, Y. Shi, C. Hao, K. Yin, and T. Zhang, Nat. Commun. **9**, 421 (2018).
[30] C. Liu, S. Lin, Y. Pei, and X. C. Zeng, J. Am. Chem. Soc. **135**, 18067 (2013).
[31] M. B. Cortie, M. J. Coutts, C. Ton-That, A. Dowd, V. J. Keast, and A. M. McDonagh, J. Phys. Chem. C **117**, 11377 (2013).
[32] S. Kundu, K. Das, and O. Konovalov, AIP Adv. **3**, 092130 (2013).
[33] R. Ristau, R. Tiruvalam, P. L. Clasen, E. P. Gorskowski, M. P. Harmer, C. J. Kiely, I. Hussain, and M. Brust, Gold Bull. (London) **42**, 133 (2009).
[34] M. P. Boneschanscher, W. H. Evers, J. J. Geuchies, T. Altantzis, B. Goris, F. T. Rabouw, S. Van Rossum, H. S. van der Zant, L. D. Siebbeles, and G. Van Tendeloo, Science **344**, 1377 (2014).
[35] H.-G. Liao, D. Zherebetskyy, H. Xin, C. Czarnik, P. Ercius, H. Elmlund, M. Pan, L.-W. Wang, and H. Zheng, Science **345**, 916 (2014).
[36] See Supplemental Material at http://link.aps.org/supplemental/10.1103/PhysRevLett.124.066101 for more detailed methods, the influence of the length of ligands, the van der Waals potential of Au atoms, the packing density of ligands, and the size of the Au NP on the coalesence, which includes Refs. [37–51].
[37] E. Pohjolainen, X. Chen, S. Malola, G. Groenhof, and H. Häkkinen, J. Chem. Theory Comput. **12**, 1342 (2016).
[38] W. L. Jorgensen, D. S. Maxwell, and J. TiradoRives, J. Am. Chem. Soc. **118**, 11225 (1996).
[39] S. Kumar, D. Bouzida, R. H. Swendsen, P. A. Kollman, and J. M. Rosenberg, J. Comput. Chem. **13**, 1011 (1992).
[40] J. S. Hub, B. L. de Groot, and D. van der Spoel, J. Chem. Theory Comput. **6**, 3713 (2010).
[41] H. F. Xu and B. J. Berne, J. Phys. Chem. B **105**, 11929 (2001).
[42] N. Winter, J. Vieceli, and I. Benjamin, J. Phys. Chem. B **112**, 227 (2008).
[43] J. Zielkiewicz, J. Chem. Phys. **123**, 104501 (2005).
[44] D. Swiatla-Wojcik, Chem. Phys. **342**, 260 (2007).
[45] F. H. Stillinger and A. Rahman, J. Chem. Phys. **60**, 1545 (1974).
[46] A. Kuffel and J. Zielkiewicz, J. Phys. Chem. B **112**, 15503 (2008).

[47] W. L. Jorgensen, J. Chandrasekhar, J. D. Madura, R. W. Impey, and M. L. Klein, J. Chem. Phys. **79**, 926 (1983).
[48] S. Herrwerth, W. Eck, S. Reinhardt, and M. Grunze, J. Am. Chem. Soc. **125**, 9359 (2003).
[49] P. Harder, M. Grunze, R. Dahint, G. M. Whitesides, and P. E. Laibinis, J. Phys. Chem. B **102**, 426 (1998).
[50] C. Zhang, A. Zhang, W. Hou, T. Li, K. Wang, Q. Zhang, J. s. M. de la Fuente, W. Jin, and D. Cui, ACS Nano **12**, 4408 (2018).
[51] T. Lahtinen, J. S. Haataja, T. R. Tero, H. Häkkinen, and O. Ikkala, Angew. Chem., Int. Ed. **55**, 16035 (2016).
[52] J. A. Lopez-Sanchez, N. Dimitratos, C. Hammond, G. L. Brett, L. Kesavan, S. White, P. Miedziak, R. Tiruvalam, R. L. Jenkins, A. F. Carley, D. Knight, C. J. Kiely, and G. J. Hutchings, Nat. Chem. **3**, 551 (2011).
[53] M. J. Abraham, T. Murtola, R. Schulz, S. Páll, J. C. Smith, B. Hess, and E. Lindahl, SoftwareX **1**, 19 (2015).
[54] H. J. C. Berendsen, J. R. Grigera, and T. P. Straatsma, J. Phys. Chem. **91**, 6269 (1987).
[55] U. Essmann, L. Perera, M. L. Berkowitz, T. Darden, H. Lee, and L. G. Pedersen, J. Chem. Phys. **103**, 8577 (1995).
[56] K. M. Salerno, D. S. Bolintineanu, J. M. D. Lane, and G. S. Grest, Phys. Rev. Lett. **113**, 258301 (2014).
[57] J. M. D. Lane and G. S. Grest, Phys. Rev. Lett. **104**, 235501 (2010).
[58] J. Park, H. Elmlund, P. Ercius, J. M. Yuk, D. T. Limmer, Q. Chen, K. Kim, S. H. Han, D. A. Weitz, and A. Zettl, Science **349**, 290 (2015).
[59] S. Maskey, J. M. D. Lane, D. Perahia, and G. S. Grest, Langmuir **32**, 2102 (2016).
[60] D. Aryal, A. Agrawal, D. Perahia, and G. S. Grest, Langmuir **33**, 11070 (2017).
[61] U. Anand, J. Lu, D. Loh, Z. Aabdin, and U. Mirsaidov, Nano Lett. **16**, 786 (2016).